Chemical Engineering Journal 488 (2024) 150833

Contents lists available at ScienceDirect

Chemical Engineering Journal

journal homepage: www.elsevier.com/locate/cej

Engineering pore limiting diameter of metal–organic frameworks for benchmark separation of mono- and di-branched hexane isomers

Jingyi Zhou [a,1], Xiao Han [a,1], Tian Ke [a], Jasper M. van Baten [b], Zongbi Bao [a,c], Zhiguo Zhang [a,c], Rajamani Krishna [b,*], Qilong Ren [a,c], Qiwei Yang [a,c,*]

[a] Key Laboratory of Biomass Chemical Engineering of Ministry of Education, College of Chemical and Biological Engineering, Zhejiang University, 310027 Hangzhou, Zhejiang, China
[b] Van't Hoff Institute for Molecular Sciences, University of Amsterdam, Science Park 904, 1098 XH Amsterdam, The Netherlands
[c] Institute of Zhejiang University-Quzhou, 324000 Quzhou, Zhejiang, China

ARTICLE INFO

Keywords:
Adsorption
Kinetic separation
Metal–organic frameworks
Hexane isomers

ABSTRACT

The separation of mono- and di-branched hexane isomers remains an important and challenging industrial process for the production of high-octane gasoline. Suitable adsorbents with high adsorption selectivity and capacity are urgently required. Herein, we demonstrate a strategy to realize highly efficient kinetically controlled hexane isomers adsorption separation that utilizes the tunability of the pore limiting diameter in M_2TTFTB (M=Zn, Mn, Cd) by metal substitution. The appropriate refinement of the partially contracted pore not only improved the kinetic selectivities, but also enhanced the host–guest interaction and increased the adsorption capacity of 3MP and nHEX. The resulting Mn_2TTFTB brought about both the record capacity of 3MP and the record kinetic selectivities of 3MP/22DMB and nHEX/22DMB, exhibiting the largest productivity of high-purity 22DMB in the breakthrough experiments, which sets a new benchmark for the hexane isomers separation via a rarely reported kinetically controlled mechanism.

1. Introduction

Within the petrochemical industry, gasoline is of particular significance because of its widespread applications in our daily life. The premium-grade gasoline not only exhibits high combustion efficiency but also has a low proclivity to detonate [1,2]. A common approach for improving gasoline quality is to increase the research octane number (RON) [3,4]. As a typical constituent of gasoline, hexane (C6) isomers are obtained from catalytic isomerization reactions of naphtha streams as a mixture and their corresponding RON values show great differences concerning their degree of branching. The linear n-hexane (nHEX), mono-branched 3-methylpentane (3MP) and di-branched 2,2-dimethylbutane (22DMB) have RON values of 30, 74.5 and 91.8, respectively [5–8]. Thus, removing alkane isomers with low RON is a crucial process to produce premium-grade gasoline.

In comparison with traditional extractive distillation and fraction crystallization, adsorption separation creates opportunities to avoid the energy-extensive separation processes based on phase changes and thus improve the separation efficiency [9–12]. However, the inert nature and similar physical properties of hexane isomers intrinsically challenge the design of suitable adsorbents. The current benchmark commercial adsorbent for this separation process is zeolite 5A, which can adsorb linear alkanes while excluding branched isomers due to suitable pore size [13–15]. However, its incapability to discriminate mono- and di-branched isomers prevents the application for further improvement of RON. Recent efforts have therefore been made to find new adsorbents with improved performance for this process.

As emerging adsorption materials, metal–organic frameworks (MOFs) feature prospective ability in engineering pore size and pore chemistry because of their modular structures [16–20]. In terms of hexane isomers, some MOFs have already realized the separation of 3MP and 22DMB with the mechanism of thermodynamic difference [21–26] or size exclusion [26–30]. Nonetheless, adsorbents in thermodynamic separation exhibit a propensity to adsorb all isomers, and thus probably

* Corresponding authors at: Key Laboratory of Biomass Chemical Engineering of Ministry of Education, College of Chemical and Biological Engineering, Zhejiang University, 310027 Hangzhou, Zhejiang, China (Q. Yang); Van't Hoff Institute for Molecular Sciences, University of Amsterdam, Science Park 904, 1098 XH Amsterdam, The Netherlands (R. Krishna).
E-mail addresses: r.krishna@contact.uva.nl (R. Krishna), yangqw@zju.edu.cn (Q. Yang).
[1] These authors contributed equally to this work.

https://doi.org/10.1016/j.cej.2024.150833
Received 6 September 2023; Received in revised form 28 February 2024; Accepted 29 March 2024
Available online 30 March 2024
1385-8947/© 2024 Published by Elsevier B.V.

result in limited separation selectivity while that in size-exclusion separation tend to exhibit low capacity due to the small-range pore size limited by the molecular size of di-branched hexane. The trade-off effect between selectivity and capacity leads to a low productivity of pure 22DMB in breakthrough experiments and becomes a significant barrier in hexane isomers separation. Kinetic separation is based on the difference in the diffusion rates of different adsorbates in the pores of adsorbents. It is capable of realizing a kinetic exclusion if the diffusion rate difference is large enough. Moreover, the corresponding pore diameter is generally larger than the molecular sizes of adsorbates, which creates opportunities to achieve higher adsorption capacity. However, pores suitable for kinetic separation are intractable to design because not only pore size and pore environment but also pore shape need to be taken into consideration for their synergistic effect on separation performance. Besides, the similar molecular size and properties of hexane isomers overweight the difficulty of adsorbent design. As a result, only a few MOFs have been reported to be used in the kinetic separation of hexane isomers, with unsatisfactory kinetic separation selectivity and small adsorption capacity [31–33]. There is still a broad space to further develop advanced adsorbents to enhance the kinetic separation and achieve 22DMB exclusion and substantial 3MP (nHEX) uptake.

Considering that channels with pore sizes too large relative to the guest molecules are unable to discriminate the diffusion rates of similar guest molecules, the construction of pores close to the size of the guest molecules is essential for efficient kinetic separation. However, due to the similar cross sections of 3MP and 22DMB molecules, a narrow normal channel that impedes the diffusion of 22DMB may also significantly impede the diffusion of 3MP and nHEX, thus harming the adsorption efficiency. The inhomogeneous zigzag channels, characterized by contoured pore surfaces and diverse pore shapes, usually exhibit significantly different pore limiting diameter (PLD) and largest cavity diameter (LCD), which conceivably provides opportunities to realize the kinetic exclusion of 22DMB by the rational refinement of PLD while maintaining the high adsorption efficiency of other isomers due to the rapid diffusion of molecules through more spacious sections (Fig. 1). Therefore, more research efforts are needed to construct zigzag channels with delicate pore structure and environment to facilitate the kinetic separation of hexane isomers with high selectivity and capacity.

Herein, we constructed a series of M_2TTFTB (M=Zn, Mn, Cd) materials with confined zigzag channels based on the tetrathiafulvalene-tetrabenzoate (H_4TTFTB) ligand, and demonstrated a strategy to realize highly efficient kinetically controlled hexane isomers separation that utilizes the tunability of pore limiting diameter (PLD) in M_2TTFTB, which brought about both record capacity of 3MP and record kinetic selectivities of 3MP/22DMB and nHEX/22DMB. Through altering the metal node from Zn to Mn and to Cd for coordinating with TTFTB, the rotation degree of metal carboxylate chains in the formed MOFs can be finely changed to construct a partially contracted pore aperture, which significantly diminished the diffusion rate of 22DMB while exhibited relatively slight effect on that of 3MP and nHEX, thus achieving an obvious improvement on the kinetic selectivities of 3MP/22DMB and nHEX/22DMB. Moreover, the appropriate refinement of the pore size from Zn_2TTFTB to Mn_2TTFTB also strengthened the host–guest interactions and increased the adsorption capacity of 3MP and nHEX, contributing to breaking the trade-off between adsorption capacity and selectivity. As a result, Mn_2TTFTB exhibited the longest gap of the retention time between di-branched and mono-branched isomers and the largest productivity of high-purity 22DMB in the breakthrough experiments among reported materials, setting a new benchmark for the hexane isomers separation.

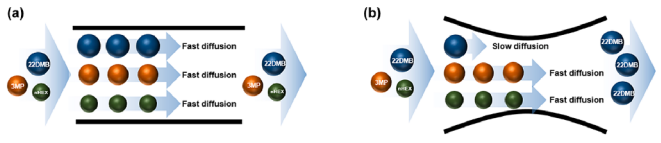

Fig. 1. Schematic diagram of the diffusion of hexane isomers in (a) homogeneously large channels and (b) inhomogeneous zigzag channels with suitable PLD.

2. Results and discussion

M_2TTFTB (M=Zn, Mn, Cd) powders were synthesized by stirring a mixed water/ethanol/*N*,*N*-dimethylformamide solution of tetrathiafulvalene-tetrabenzoate (H_4TTFTB) and different metal nitrates at 348 K for 3 days [34,35]. Powder X-ray diffraction patterns (PXRD) revealed that M_2TTFTB samples were of high crystallinity and isostructural with each other (Figs. S1–S4). The infinite helical chains of corner-sharing MO_6 pseudo-octahedra were interconnected by TTFTB ligands, forming three-dimensional structures that crystalized in the hexagonal space group *P*65. After desolvation under high vacuum (<1 Pa) at 393 K, solvents and coordinated water molecules were removed as indicated by the thermogravimetric analysis (TGA). As shown in Fig. 2, M2TTFTB (M=Zn, Mn, Cd) exhibited tortuous zigzag channels along the c axis, and adjacent channels were linked by connecting channels to form a three-dimensional mesh-like porous network. Through altering the metal node from Zn to Mn and Cd with a larger atom radius, the metal carboxylate chains in the formed MOFs can be finely changed to be more distorted. The angles between adjacent metal atoms are 165.9°, 151.2°, and 143.9° (Fig. S5), respectively, resulting in the gradually aggravated rotation of the benzene rings of TTFTB ligands. This contributes to the precise refinement of the aperture size in some sections of the channels. As shown in Fig. 3, the closest distances between hydrogen atoms of the benzene rings on opposite sides of the channel along the c axis in Zn_2TTFTB are 6.78 and 7.11 Å, which determines the limiting aperture size in the channel. These H···H distances are reduced to 6.50 and 7.01 Å in Mn_2TTFTB, and 6.45 and 6.78 Å in Cd_2TTFTB, implying that the limiting aperture size along the c axis follows the order of Zn_2TTFTB > Mn_2TTFTB > Cd_2TTFTB. However, the distances between carbon atoms on opposite sides of the connecting channel exhibited a different order, which on average is 8.39 Å in Zn_2TTFTB, 8.16 Å in Mn_2TTFTB, and 8.28 Å in Cd_2TTFTB, implying that the limiting aperture size of connecting channels followed the order of Zn_2TTFTB > Cd_2TTFTB > Mn_2TTFTB. Besides, the LCD (largest cavity diameter) and PLD (pore limiting diameter) of the entire framework were calculated by Zeo++ package with a probe radius of 1.82 Å. The LCD of Cd_2TTFTB (5.61 Å) is larger than that of Zn_2TTFTB (5.45 Å) and Mn_2TTFTB (5.39 Å) while its PLD is the smallest (4.47 Å vs. 4.63 Å in Zn_2TTFTB and 4.50 Å in Mn_2TTFTB). According to the above analysis, the PLD is believed to correspond to the limiting aperture size along the c axis that also followed the order of Zn_2TTFTB > Mn_2TTFTB > Cd_2TTFTB.

The BET surface areas of M_2TTFTB (M=Zn, Mn, Cd) determined from the 77 K N_2 adsorption isotherms were 699, 688, and 592 m^2/g (Figs. S6–S11). TGA revealed that they were stable until 440 °C, 470 °C and 380 °C (Figs. S12–S14). In situ variable-temperature PXRD indicated that they maintained their original crystal structures at high temperature up to at least 423 K. (Figs. S15–17) Guest-atmosphere TGA showed that the nHEX uptake capacity of Mn_2TTFTB remained unchanged after 30 consecutive adsorption–desorption cycles at 333 K (Fig. 4d), indicating its adsorption recyclability. Moreover, there was no detectable change in either crystallinity or porosity of these samples after exposure to air for one week, as evidenced by the retained peaks and relative intensities in their corresponding PXRD patterns as well as the retained porosity (Figs. S18–S20).

To investigate the adsorption behavior of hexane isomers on M_2TTFTB (M=Zn, Mn, Cd), single-component adsorption isotherms of nHEX, 3MP and 22DMB were measured at 303 K, 333 K, 363 K and 393 K, respectively. Zn_2TTFTB exhibited very steep adsorption isotherms, with adsorption capacities of 1.86 mmol/g (9.1 molecule/cell) for nHEX, 2.01 mmol/g (9.9 molecule/cell) for 3MP and 1.88 mmol/g (9.3 molecule/cell) for 22DMB at 303 K and 100 torr, respectively (Figs. S21-

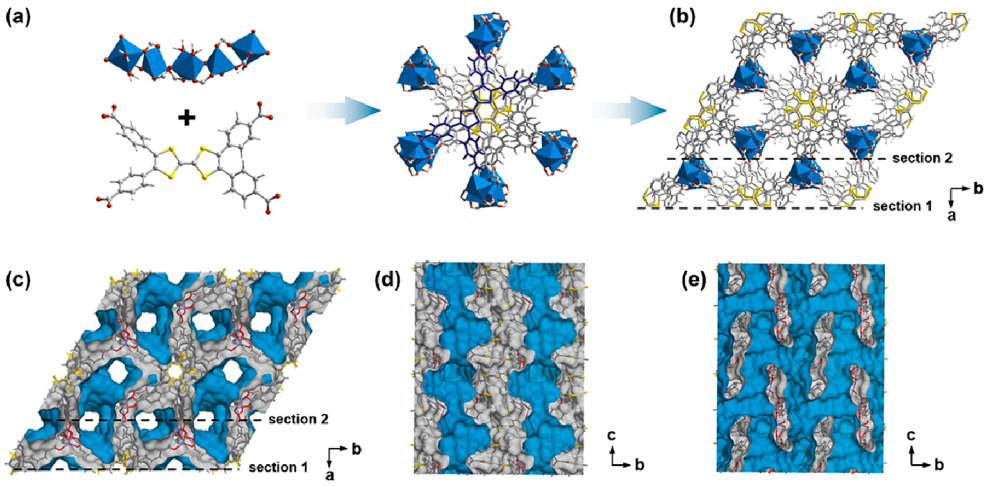

Fig. 2. Structural illustration of M_2TTFTB (M=Zn, Mn, Cd): (a) The coordination between the infinite helical chains of corner-sharing MO_6 pseudo-octahedra and TTFTB ligands (one TTFTB molecule was highlighted in violet for clarity); (b) The structure of M_2TTFTB (M=Zn, Mn, Cd); Structural cross sections with Connolly surface with probe radius of 1 Å: (c) on ab plane; (d) on bc plane and corresponded to section 1; (e) on bc plane and corresponded to section 2. (For interpretation of the references to colour in this figure legend, the reader is referred to the web version of this article.)

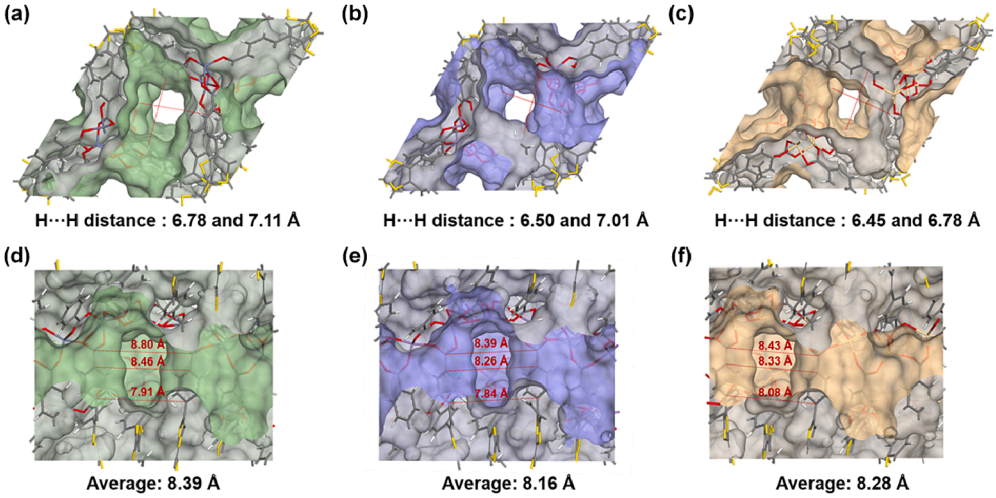

Fig. 3. Schematic diagram of the closest distances between hydrogen atoms of the benzene rings on opposite sides of the channel along the c axis: (a) Zn_2TTFTB; (b) Mn_2TTFTB; (c) Cd_2TTFTB; Distances between carbon atoms on opposite sides of the connecting channel: (d) Zn_2TTFTB; (e) Mn_2TTFTB; (f) Cd_2TTFTB.

S23). Their adsorption amounts all decreased with the increase in temperature. Mn_2TTFTB also showed steep isotherms of nHEX and 3MP, but with significantly higher adsorption capacities than that in Zn_2TTFTB (Fig. 4a and 4b), reaching 2.11 mmol/g (10.0 molecule/cell) and 2.41 mmol/g (11.5 molecule/cell). It is worth noting that its nHEX adsorption capacity is 74 % larger than that of zeolite 5A (1.21 mmol/g), and its 3MP adsorption capacity exceeds all the reported materials (Table S1). Meanwhile, the isotherms of 22DMB were relatively flatter. Its adsorption capacity was 0.65 mmol/g (3.4 molecule/cell) at 303 K (Fig. 4c), significantly lower than that of nHEX and 3MP. Interestingly, with the increase in temperature, the adsorption capacity of 22DMB first increased and then decreased in the order of 333 K > 363 K > 393 K > 303 K, which was probably related to the diffusion restriction of adsorbates at low temperatures and the setup of the test instrument. The adsorption isotherms of Cd_2TTFTB were similar to those of Mn_2TTFTB, but the adsorption capacities of nHEX and 3MP were significantly reduced, 1.45 mmol/g (7.9 molecule/cell) and 1.72 mmol/g (9.3 molecule/cell), respectively (Fig. 4e and Fig. S24). With the increase of temperature, the capacity of 22DMB followed the order of 363 K > 333 K > 393 K > 303 K, and was 0.84 mmol/g (4.71 molecule/cell) at 303 K (Fig. 4f), implying the more restricted diffusion process of 22DMB in Cd_2TTFTB. The distinction of M_2TTFTB (M=Zn, Mn, Cd) materials with different metal sites in single-component static adsorption demonstrated the prominent effect of the metal substitution, inspiring us to conduct further experiments to verify their separation performance and clarify the separation mechanism.

To have a deeper insight into the adsorption behaviors of hexane isomers, we also performed kinetics studies to verify the mass-transfer rate of hexane isomers in M_2TTFTB using volumetric methods. The diffusion time constant (D_c/r^2, s^{-1}) was obtained by fitting the kinetics curves according to the following equation:[36]

$$\frac{m_t}{m_\infty} = \frac{6}{\sqrt{\pi}}\sqrt{\frac{D_c}{r_c^2}t} - 3\frac{D_c}{r_c^2}t \quad (1)$$

where m_t/m_∞ is the fractional adsorption uptake at time t; D_c is the intracrystalline diffusivity; r_c is the radius of the equivalent spherical particle.

As shown in Fig. 5a, three hexane isomers exhibited a discrepancy in diffusion rates, which followed the trend nHEX > 3MP > 22DMB in all M_2TTFTB materials. Among them, guest molecules diffused quickly in Zn_2TTFTB with the largest PLD. nHEX exhibited a short equilibrium

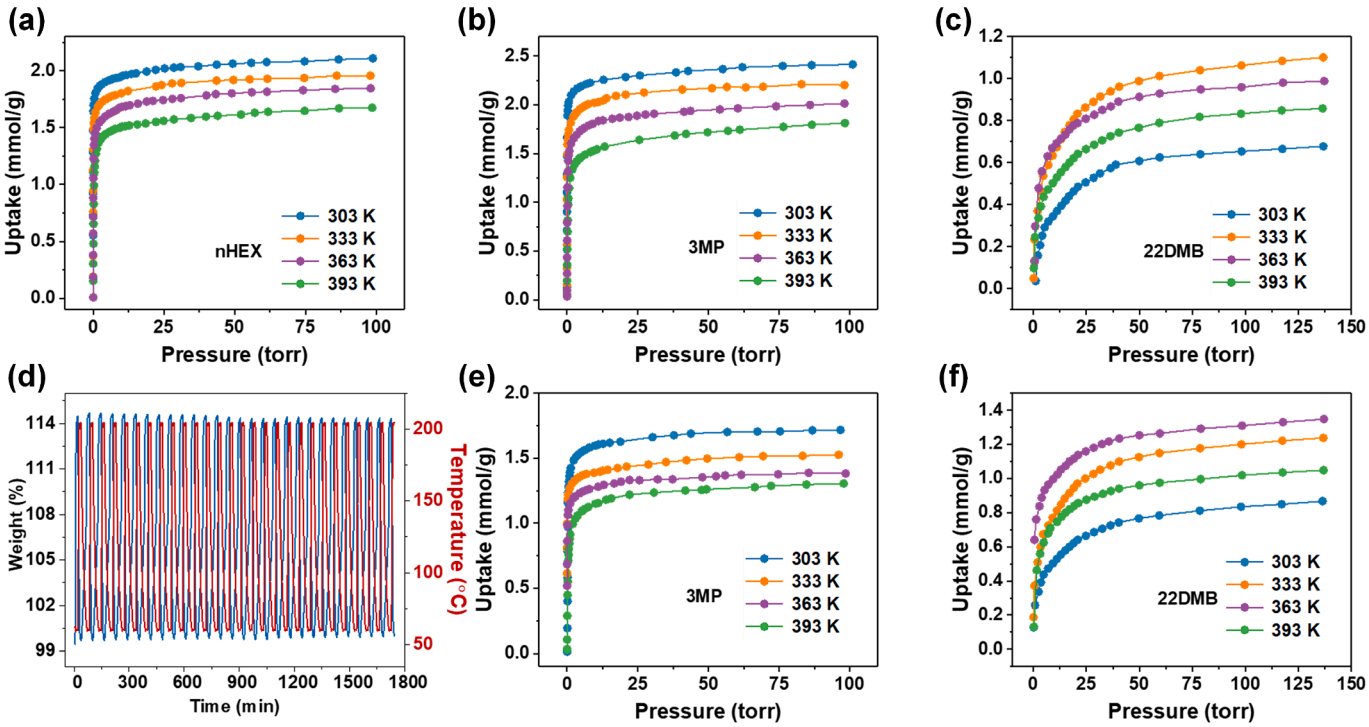

Fig. 4. Adsorption isotherms of (a) nHEX, (b) 3MP, and (c) 22DMB for Mn_2TTFTB at different temperatures; (d) nHEX adsorption–desorption recyclability test on Mn_2TTFTB for 30 consecutive adsorption cycles at 333 K; Adsorption isotherms of (e) 3MP, and (f) 22DMB for Cd_2TTFTB at different temperatures.

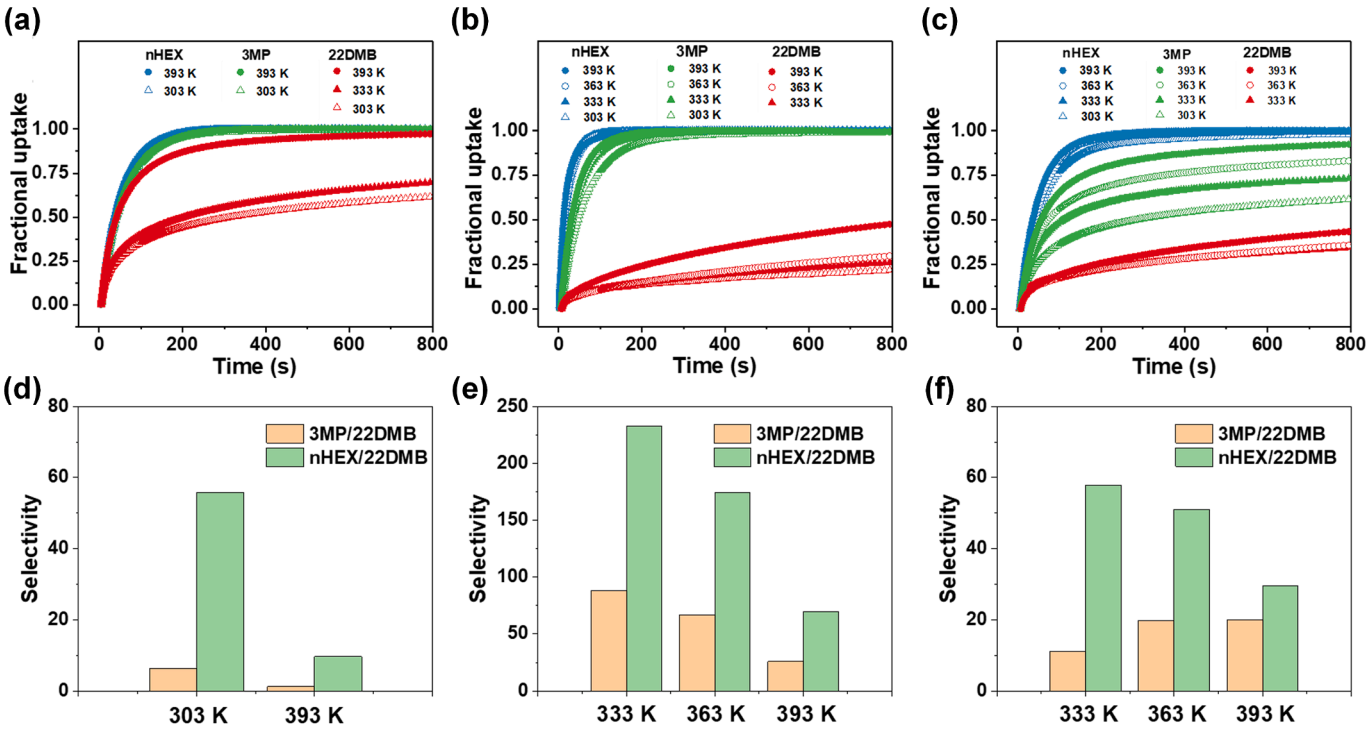

Fig. 5. Fractional uptake profiles of nHEX, 3MP and 22DMB for (a) Zn_2TTFTB, (b) Mn_2TTFTB, and (c) Cd_2TTFTB; Kinetic selectivities of 3MP/22DMB and nHEX/22DMB in (d) Zn_2TTFTB, (e) Mn_2TTFTB, and (f) Cd_2TTFTB.

time of about 1 min at 303 K while 3MP and 22DMB diffused slightly slower with an equilibrium time of 6 min and 15 min, respectively. Their diffusion time constants (D_c/r^2) were calculated to be 59.90 × 10^{-4}, 6.87 × 10^{-4} and 1.08 × 10^{-4} s^{-1}, respectively (Fig. S25). With the increase of temperature, their diffusion was all accelerated, and the diffusion time constants of 3MP and 22DMB were very close (8.71 × 10^{-4} and 7.00 × 10^{-4} s^{-1}) at 393 K, resulting in a low 3MP/22DMB kinetic selectivity (Fig. 5d). In Mn_2TTFTB and Cd_2TTFTB, the diffusion rates of guest molecules were all reduced (Fig. 5b and 5c). The diffusion time constants of nHEX and 3MP in Mn_2TTFTB were 22.96 × 10^{-4} and 8.49 × 10^{-4} s^{-1}, and in Cd_2TTFTB were 7.34 × 10^{-4} and 5.00 × 10^{-4} at 393 K, respectively (Figs. S26 and S27). Meanwhile, 22DMB diffused

much slower so that more than 200 and 400 min were needed to reach equilibrium in Mn_2TTFTB and Cd_2TTFTB even at 393 K, with a diffusion rate constant of 0.33 × 10^{-4} and 0.25 × 10^{-4} s^{-1}, respectively. The activation energies were found to be 2.5, 5.7 and 23.1 kJ/mol for nHEX, 3MP and 22DMB in Mn_2TTFTB, and 2.6, 18.3 and 27.9 kJ/mol in Cd_2TTFTB, respectively (Fig. S28). The most pronounced diffusion limitation of isomers in Cd_2TTFTB with the smallest PLD but the largest LCD among the three MOFs implied the dominant role of PLD in the kinetic separation performance. The kinetic selectivities of nHEX/22DMB and 3MP/22DMB in Cd_2TTFTB were 28.93 and 20.11, and in Mn_2TTFTB were 25.81 and 69.81 at 393 K (Fig. 5e and 5f), which were not only higher than those in Zn_2TTFTB but also surpassed other reported materials capable of separating hexane isomers based on a kinetic mechanism. As the temperature decreased, the kinetic selectivity of 3MP/22DMB in Cd_2TTFTB decreased to 11.05 at 333 K. However, the kinetic selectivities of both nHEX/22DMB and 3MP/22DMB in Mn_2TTFTB were further increased and reached 88.00 and 232.47 at 333 K, which was probably due to the appropriate PLD of Mn_2TTFTB that significantly decreased the diffusion rate of 22DMB while exhibiting relatively little effect on that of 3MP and nHEX, setting new records for kinetic selectivities.

To estimate the practical separation performance of M_2TTFTB materials, equimolar three-component vapor-phase breakthrough tests with partial pressure of 47 torr for each isomer were carried out at 303 K, 333 K, 363 K and 393 K. In the ternary breakthrough test on Zn_2TTFTB at 303 K, 22DMB was retained for 107 min/g before eluted from the column, followed by 3MP (152 min/g) and then nHEX (291 min/g), indicating a successful separation among the di-branched, mono-branched, and linear isomers (Fig. S29). However, the separation ability of Zn_2TTFTB decreased obviously at 393 K with three isomers eluting almost simultaneously (Fig. S30). In Mn_2TTFTB, 22DMB were barely adsorbed and broke through the column immediately at 303 K, 333 K and 363 K (Fig. 6a, 6b, and S31). Although the single-component isotherms indicated a large adsorption capacity of 22DMB in Mn_2TTFTB (eg. 333 K: 1.06 mmol/g), its low diffusion rate prevented it from diffusing rapidly into the pores, thus realizing the dynamic exclusion of 22DMB in the breakthrough experiment under these circumstances. When the temperature rose to 393 K, the diffusion of 22DMB became faster, and some of them were adsorbed by Mn_2TTFTB with a breakthrough time of 15 min/g, but the dynamic adsorption capacity was still significantly smaller than the corresponding static adsorption capacity (0.0046 mmol/g vs. 0.83 mmol/g). 3MP was substantially adsorbed by Mn_2TTFTB and eluted secondly (Fig. 6c). With increasing temperature, its retention time initially increased and then decreased, which was 77 min/g at 303 K, 190 min/g at 333 K, 135 min/g at 363 K, and 92 min/g at 393 K, respectively. It is well known that the adsorption separation process is under the control of both thermodynamics and kinetics factors. The temperature rise increased the adsorption rate (kinetics) but decreased the adsorption capacity at equilibrium (thermodynamics). The low diffusion rate of 3MP, as indicated by the above kinetics studies, made the dynamic adsorption process evidently restricted at lower temperatures, thus resulting in the abnormal trend of the retention time over temperature and its earlier elution than nHEX. Meanwhile, the same trend was also observed for nHEX. Its retention time at 303 K, 333 K, 363 K and 393 K was 144 min/g, 320 min/g, 239 min/g and 222 min/g, respectively, indicating again the dominant role of kinetic factors in the separation. It's worth noting that Mn_2TTFTB exhibited a long retention time gap between di-branched and mono-branched isomers at 333 K (180 min/g) with a productivity of high-purity 22DMB (≥99.8 % purity) reaching 0.45 mmol/g, exceeding all previously reported adsorbents under the same conditions (Table S1 and S2).

In Cd_2TTFTB, 22DMB can also be dynamically excluded at 303, 333, and 363 K while 3MP and nHEX were both adsorbed (Fig. 6d, 6e, and S32). However, the retention time of 3MP at 303 K was only 36 min/g, much shorter than that in Mn_2TTFTB. Moreover, the breakthrough curves of 3MP in Cd_2TTFTB rose more slowly than that in Mn_2TTFTB, suggesting a slower diffusion in Cd_2TTFTB. With the increase in temperature, the retention time of 3MP first increased to 53 min/g at 333 K and 164 min/g at 363 K, and then decreased to 92 min/g at 393 K (Fig. 6f). The best separation performance was obtained at 363 K, with a record retention time gap between 3MP and 22DMB of 146 min/g and a

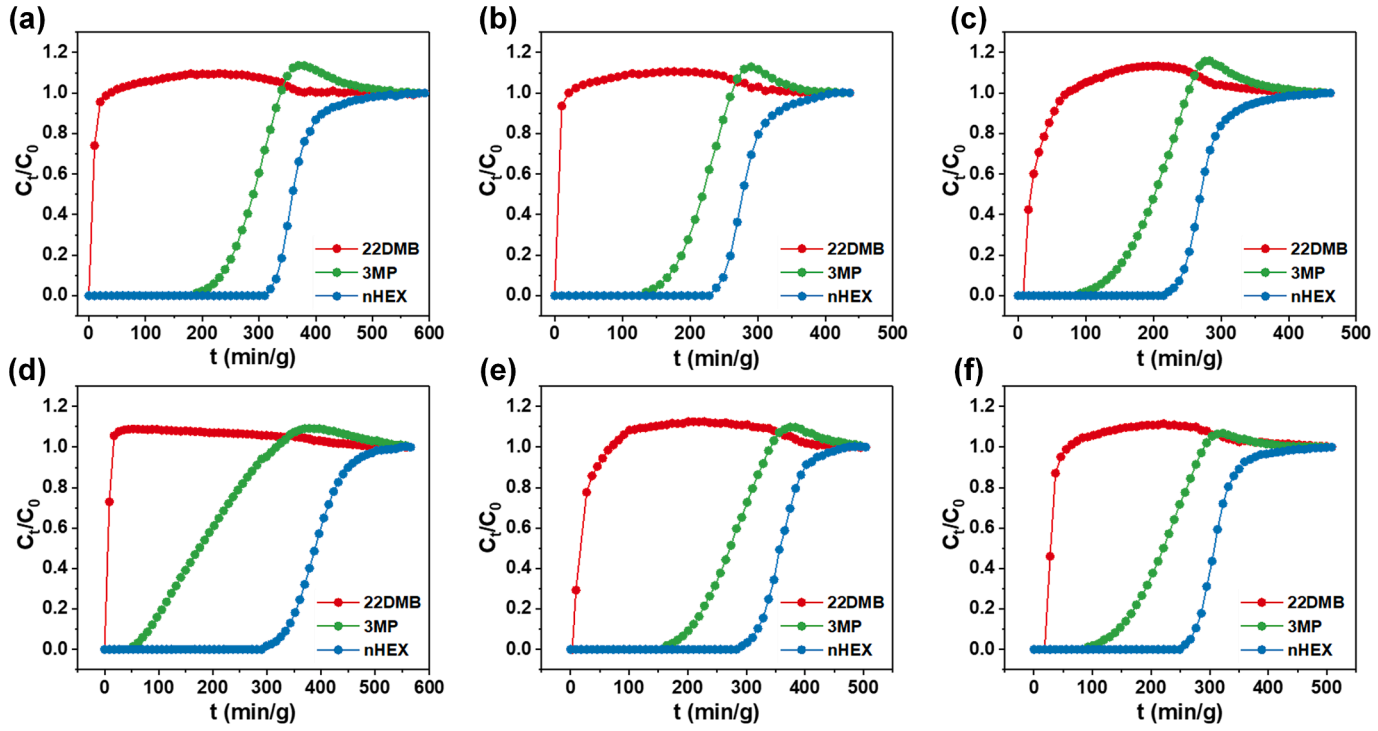

Fig. 6. Equimolar three-component vapor-phase breakthrough curves of Mn_2TTFTB at (a) 333 K, (a) 363 K, (a) 393 K, and of Cd_2TTFTB at (d) 333 K, (e) 363 K, (f) 393 K.

record 22DMB productivity (≥99.8 % purity) of 0.36 mmol/g among all the reported materials under the same conditions (Table S1 and S2). In addition, the desorption tests of the Mn_2TTFTB and Cd_2TTFTB were carried out after the breakthrough tests at 393 K (Figs. S33 and S34). With a flow rate of 5 mL/min N_2 introduced, both 3MP and nHEX can be fully desorbed at 423 K within 300 min/g. Furthermore, multiple breakthrough tests revealed that Mn_2TTFTB and Cd_2TTFTB maintained their separation performance after seven cycles, indicating their dynamic recyclability and stability (Figs. S35 and S36).

Dispersion-corrected density functional theory (DFT-D) calculations were further performed to explore the preferred adsorption sites of hexane isomers in the channels of M_2TTFTB (M=Zn, Mn, Cd) materials. As shown in Fig. 7, all of the isomers tended to locate in the larger aperture and close to the metal carboxylate chains. In all M_2TTFTB materials, the binding energy of different hexane isomers followed the trend nHex > 3MP > 22DMB, but the discrepancy was small (lower than 8 kJ/mol). The slender nHex molecules were arranged along the metal carboxylate chains and interacted with the surrounding oxygen atoms through multiple C—H···O dipolar interactions. The mono-branched 3MP and di-branched 22DMB molecules exhibited shorter but less C—H···O bonds due to their bulgier size, resulting in slightly lower static adsorption energy (Table S3) than nHEX. Besides, it is worth noting that from Zn_2TTFTB to Mn_2TTFTB, the appropriate refinement of the pore size contributed to denser C—H···O interactions between the metal carboxylate chains and the hexane isomers, and thus strengthened their binding energy. However, from Mn_2TTFTB to Cd_2TTFTB, the pore space was too restricted to further enhance the host–guest interaction, resulting instead in a marginal decrease in the binding energy. Overall, these slight discrepancies in the static adsorption energy of different hexane isomers contributed to some extent to the excellent separation performance of Mn_2TTFTB and Cd_2TTFTB, but were not the reason that endowed them with outstanding separation selectivities in breakthrough experiments, further indicating the important role that different diffusion behaviors of hexane isomers played in the separation.

3. Conclusion

This study demonstrates that tuning the PLD by metal substitution offers a viable strategy to realize highly efficient kinetically controlled hexane isomers adsorption separation. The resulting MOF, Mn_2TTFTB exhibited record adsorption capacity of 3MP, record kinetic selectivities of 3MP/22DMB and nHEX/22DMB, and record 22DMB productivity in the equimolar ternary breakthrough experiments. The appropriate refinement of the partially contracted pores not only contributed to denser C—H···O interactions, ensuring that C6 molecules were effectively grasped within the framework, but also provided opportunities to realize the kinetic exclusion of 22DMB, achieving an obvious improvement in kinetic selectivities without the expense of adsorption capacity.

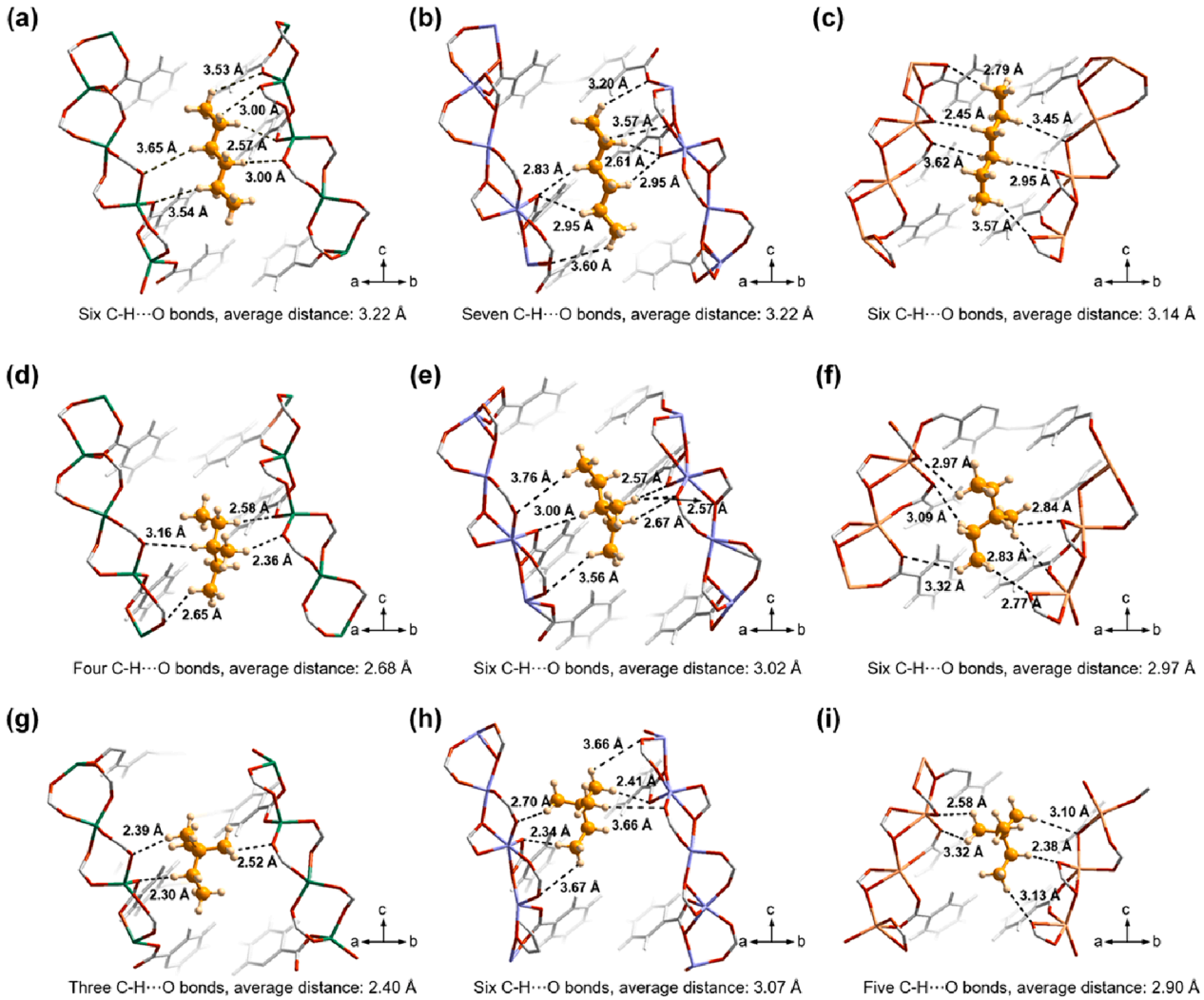

Fig. 7. Preferred adsorption sites by DFT-D simulations. nHEX adsorption sites in (a) Zn_2TTFTB, (b) Mn_2TTFTB, and (c) Cd_2TTFTB; 3MP adsorption sites in (d) Zn_2TTFTB, (e) Mn_2TTFTB, and (f) Cd_2TTFTB; 22DMB adsorption sites in (g) Zn_2TTFTB, (h) Mn_2TTFTB, and (i) Cd_2TTFTB.

This work not only offers the strategy for refining PLD of porous adsorbents by metal substitution, but also indicates that PLD is critical for efficient kinetic separation, encouraging researchers to apply it to other kinetic separations of mixtures with similar structures and properties.

CRediT authorship contribution statement

Jingyi Zhou: Writing – original draft, Investigation, Formal analysis. **Xiao Han:** Investigation, Writing – original draft, Data curation. **Tian Ke:** Writing – review & editing, Investigation. **Jasper M. van Baten:** Visualization, Software. **Zongbi Bao:** Resources, Validation, Formal analysis. **Zhiguo Zhang:** Resources, Project administration. **Rajamani Krishna:** Visualization, Software, Conceptualization. **Qilong Ren:** Funding acquisition, Conceptualization. **Qiwei Yang:** Conceptualization, Writing – review & editing, Funding acquisition, Project administration, Formal analysis, Data curation.

Declaration of competing interest

The authors declare that they have no known competing financial interests or personal relationships that could have appeared to influence the work reported in this paper.

Data availability

Data will be made available on request.

Acknowledgments

This work was supported by the Zhejiang Provincial Natural Science Foundation of China (LR21B060002), the National Natural Science Foundation of China (No. 22178305, 21890764, 22293061 and 22288102) and the Fundamental Research Funds for the Central Universities (2021FZZX001-15).

Appendix A. Supplementary data

Supplementary data to this article can be found online at https://doi.org/10.1016/j.cej.2024.150833.

References

[1] R.A. Myers, Handbook of petroleum refining processes, McGraw-Hill, New York, 2004.
[2] R. Vismara, C. Di Nicola, R.G.S. Millán, K.V. Domasevich, C. Pettinari, J. A. Navarro, Efficient hexane isomers separation in isoreticular bipyrazolate metal–organic frameworks: the role of pore functionalization, S. Galli, Nano Res. 14 (2020) 532–540.
[3] H. Wang, Y. Liu, J. Li, Designer metal–organic frameworks for size-exclusion-based hydrocarbon separations: progress and challenges, Adv. Mater. 32 (2020) 2002603.
[4] Z. Zhang, S.B. Peh, C. Kang, K. Chai, D. Zhao, Metal–organic frameworks for C6–C8 hydrocarbon separations, EnergyChem 3 (2021) 100057.
[5] S. Mukherjee, A.V. Desai, S.K. Ghosh, Potential of metal–organic frameworks for adsorptive separation of industrially and environmentally relevant liquid mixtures, Coord. Chem. Rev. 367 (2018) 82–126.
[6] Z. Bao, G. Chang, H. Xing, R. Krishna, Q. Ren, B. Chen, Potential of microporous metal–organic frameworks for separation of hydrocarbon mixtures, Energy Environ. Sci. 9 (2016) 3612–3641.
[7] H. Wang, J. Li, Microporous metal–organic frameworks for adsorptive separation of C5–C6 alkane isomers, Accounts Chem. Res. 52 (2019) 1968–1978.
[8] R. Krishna, J.M. van Baten, Screening metal–organic frameworks for separation of pentane isomers, Phys. Chem. Chem. Phys. 19 (2017) 8380–8387.
[9] J. Zhou, T. Ke, F. Steinke, N. Stock, Z. Zhang, Z. Bao, X. He, Q. Ren, Q. Yang, Tunable confined aliphatic pore environment in robust metal–organic frameworks for efficient separation of gases with a similar structure, J. Am. Chem. Soc. 144 (2022) 14322–14329.
[10] P.J. Bereciartua, A. Cantin, A. Corma, J.L. Jorda, M. Palomino, F. Rey, S. Valencia, E.W. Corcoran, P. Kortunov, P.I. Ravikovitch, Control of zeolite framework flexibility and pore topology for separation of ethane and ethylene, Science 358 (2017) 1068–1071.
[11] A. Torres-Knoop, R. Krishna, D. Dubbeldam, Separating xylene isomers by commensurate stacking of p-xylene within channels of MAF-X8, Angew. Chem. Int. Edit. 53 (2014) 7774–7778.
[12] D.S. Sholl, R.P. Lively, Seven chemical separations to change the world, Nature 532 (2016) 435–437.
[13] D. Peralta, G. Chaplais, Simon-Masseron, A.K. Barthelet, G.D. Pirngruber, Separation of C6 paraffins using zeolitic imidazolate frameworks: Comparison with zeolite 5A, Ind. Eng. Chem. Res. 51 (2012) 4692–4702.
[14] F. Miano, Adsorption of hydrocarbon vapour mixtures onto zeolite 5A, Colloid Surf. A-Physicochem. Eng. Asp. 110 (1996) 95–104.
[15] A. Luna-Triguero, P. Gomez-Alvarez, S. Calero, Adsorptive process design for the separation of hexane isomers using zeolites, Phys. Chem. Chem. Phys. 19 (2017) 5037–5042.
[16] D. Banerjee, C.M. Simon, S.K. Elsaidi, M. Haranczyk, P.K. Thallapally, Xenon gas separation and storage using metal–organic frameworks, Chem 4 (2018) 466–494.
[17] M.I.H. Mohideen, R.S. Pillai, K. Adil, P.M. Bhatt, Y. Belmabkhout, A. Shkurenko, G. Maurin, M. Eddaoudi, A fine-tuned MOF for gas and vapor separation: a multipurpose adsorbent for acid gas removal, dehydration, and BTX sieving, Chem 3 (2017) 822–833.
[18] D.-D. Zhou, P. Chen, C. Wang, S.-S. Wang, Y. Du, H. Yan, Z.-M. Ye, C.-T. He, R.-K. Huang, Z.-W. Mo, N.-Y. Huang, J.-P. Zhang, Intermediate-sized molecular sieving of styrene from larger and smaller analogues, Nat. Mater. 18 (2019) 994–998.
[19] W.G. Cui, T.L. Hu, X.H. Bu, Metal–organic framework materials for the separation and purification of light hydrocarbons, Adv. Mater. 32 (2019) 1806445.
[20] J.-R. Li, R.J. Kuppler, H.-C. Zhou, Selective gas adsorption and separation in metal–organic frameworks, Chem. Soc. Rev. 38 (2009) 1477–1504.
[21] Z.R. Herm, B.M. Wiers, J.A. Mason, J.M. van Baten, M.R. Hudson, P. Zajdel, C. M. Brown, N. Masciocchi, R. Krishna, J.R. Long, Separation of hexane isomers in a metal–organic framework with triangular channels, Science 340 (2013) 960–964.
[22] Y. Ling, Z.X. Chen, F.P. Zhai, Y.M. Zhou, L.H. Weng, D.Y. Zhao, A zinc(II) metal–organic framework based on triazole and dicarboxylate ligands for selective adsorption of hexane isomers, Chem. Commun. 47 (2011) 7197–7199.
[23] H. Belarbi, L. Boudjema, N. Shepherd, G. Ramsahye, J.-S. Toquer, P.T. Chang, Adsorption and separation of hydrocarbons by the metal organic framework MIL-101(Cr), Colloid Surf. A-Physicochem. Eng. Asp. 520 (2017) 46–52.
[24] N.A. Ramsahye, P. Trens, C. Shepherd, P. Gonzalez, T.K. Trung, F. Ragon, C. Serre, The effect of pore shape on hydrocarbon selectivity on UiO-66(Zr), HKUST-1 and MIL-125(Ti) metal organic frameworks: insights from molecular simulations and chromatography, Microporous Mesoporous Mat. 189 (2014) 222–231.
[25] B. Chen, C. Liang, J. Yang, D.S. Contreras, Y.L. Clancy, E.B. Lobkovsky, O.M. Yaghi, S. Dai, A microporous metal–organic framework for gas-chromatographic separation of alkanes, Angew. Chem. Int. Edit. 45 (2006) 1390–1393.
[26] H. Wang, X. Dong, J. Lin, S.J. Teat, S. Jensen, J. Cure, E.V. Alexandrov, Q. Xia, K. Tan, Q. Wang, D.H. Olson, D.M. Proserpio, Y.J. Chabal, T. Thonhauser, J. Sun, Y. Han, J. Li, Topologically guided tuning of Zr-MOF pore structures for highly selective separation of C6 alkane isomers, Nat. Commun. 9 (2018) 1745.
[27] L. Yu, X. Dong, Q. Gong, S.R. Acharya, Y. Lin, H. Wang, Y. Han, T. Thonhauser, J. Li, Splitting mono- and dibranched alkane isomers by a robust aluminum-based metal–organic framework material with optimal pore dimensions, J. Am. Chem. Soc. 142 (2020) 6925–6929.
[28] L. Yu, S. Ullah, K. Zhou, Q. Xia, H. Wang, S. Tu, J. Huang, H.L. Xia, X.Y. Liu, T. Thonhauser, A microporous metal–organic framework incorporating both primary and secondary building units for splitting alkane isomers, J. Am. Chem. Soc. 144 (2022) 3766–3770.
[29] H. Wang, X. Dong, E. Velasco, D.H. Olson, Y. Han, J. Li, One-of-a-kind: a microporous metal–organic framework capable of adsorptive separation of linear, mono- and di-branched alkane isomers via temperature- and adsorbate-dependent molecular sieving, Energy Environ. Sci. 11 (2018) 1226–1231.
[30] E. Velasco, S. Xian, H. Wang, S.J. Teat, D.H. Olson, K. Tan, S. Ullah, T.M. Osborn Popp, A.D. Bernstein, K.A. Oyekan, Flexible Zn-MOF with rare underlying scu topology for effective separation of C6 alkane isomers, ACS Appl. Mater. Interfaces 13 (2021) 51997–52005.
[31] D. Lv, H. Wang, Y. Chen, F. Xu, R. Shi, Z. Liu, X. Wang, S.J. Teat, Q. Xia, Z. Li, Iron-based metal–organic framework with hydrophobic quadrilateral channels for highly selective separation of hexane isomers, ACS Appl. Mater. Interfaces 10 (2018) 6031–6038.
[32] P.A.P. Mendes, P. Horcajada, S. Rives, H. Ren, A.E. Rodrigues, T. Devic, E. Magnier, P. Trens, H. Jobic, J. Ollivier, G. Maurin, C. Serre, J.A.C. Silva, A complete separation of hexane isomers by a functionalized flexible metal organic framework, Adv. Funct. Mater. 24 (2014) 7666–7673.
[33] P.A.P. Mendes, A.E. Rodrigues, P. Horcajada, J. Eubank, T. Devic, C. Serre, J.A. C. Silva, Separation of hexane isomers on rigid porous metal carboxylate-based metal–organic frameworks, Adsorpt. Sci. Technol. 32 (2014) 475–488.
[34] T.C. Narayan, T. Miyakai, S. Seki, M. Dinca, High charge mobility in a tetrathiafulvalene-based microporous metal–organic framework, J. Am. Chem. Soc. 134 (2012) 12932–12935.
[35] S.S. Park, E.R. Hontz, L. Sun, C.H. Hendon, A. Walsh, T. Van Voorhis, M. Dinca, Cation-dependent intrinsic electrical conductivity in isostructural tetrathiafulvalene-based microporous metal–organic frameworks, J. Am. Chem. Soc. 137 (2015) 1774–1777.
[36] Z. Bao, S. Alnemrat, L. Yu, I. Vasiliev, Q. Ren, X. Lu, S. Deng, Adsorption of ethane, ethylene, propane, and propylene on a magnesium-based metal–organic framework, Langmuir 27 (2011) 13554–13562.